Implication of Phase-folded Diagrams for Validation of the Nature of Stellar Variability I: the case of NGC 6866

Gireesh C. Joshi[1]
Department of Physics, Government Degree College (Kotdwar Bhabar), Pauri Garwal, Uttrakhand (India)
gchandra.2012@rediffmail.com
(Submitted on 30.07.2021; Accepted on 20.09.2021)

Abstract. A membership analysis of known variable stars in the NGC 6866 open cluster indicates that the field and member stars are the red-component-stars (RCS) and blue component stars (BCS), respectively. The visual inspection of phase diagrams of alias frequencies or noise indicates no sign of regular shape of pulsation in the variable stars. Analysis of phase diagrams and frequency spectrum of variable stars, (namely, ID 00016, ID 1077, ID 1088, ID 1292, ID 1421, ID 1583 and ID 1274) of NGC 6866 confirms the detection impossibility of stellar pulsation for frequencies higher than 100 cd^{-1}. A temporal analysis of the higher frequency spectrum of each variable was performed for computing the largest amplitude of regular fluctuations. In the lower frequency spectrum ($0 \leq 100\ cd^{-1}$), there is no evidence of pulsation of the variables below this largest amplitude of regular fluctuations. The variable ID 1077 has the characteristics of SX Phoenicis and is located beyond the cluster NGC 6866.
Key words: Galaxy: open star cluster individual: NGC 6866 variables: pulsation method: data analysis

1 Introduction

Stars over essentially the whole mass domain can become pulsationally unstable during various stages of their evolution (Gautschy & Saio 1996), leading to changes in their brightness with time. A star can show various pulsating cycles either at a given stage of stellar evolution, or in the time scale of its evolution. The time scale of the pulsations and that of the stellar evolution are very different from each other. For instance, Delta Scuti stars or Classical Cepheids etc., do not show their various stages of evolution during their pulsation cycles. Groups of the cepheids and cepheid-like variables have several kind of variables and are found in the instability strip of the colour-magnitude diagram (CMD). Moreover, their pulsation variability is due to those certain conditions, which translate into the various instability strips in the Hertzsprung-Russell (HR) diagram or CMD. HR-diagram is mostly oriented towards the photometric variability (Eyer & Mowlavi 2008). Different types of B stars co-exist at the same position of the HR diagram, which coincide with the instability strip of slowly pulsating B (SPB) stars (Briquet *et al.* 2007). The period limit of eclipsing binaries is still an open issue, and may need revolutionary revision for documentation of very short period systems (Liu *et al.* 2015). The analysis of associated frequencies of detected pulsation modes of each type of variable may offer a unique opportunity to understand the internal structure of that variable (Mowlavi *et al.* 2013). These pulsation modes are an important probe to trace the physical properties of variables, including their masses, luminosities, temperatures and metallicity (Salmanzadeh *et al.* 2015). Furthermore, these pulsating variables cover a broad range of stellar-parameters and associated evolutionary stages (Derekas *et al.* 2009).

Open star clusters (OSC) are hosts of many types of variable stars (δ-Scuti, γ-Doradus, rotational, elliptical etc.,). Study of the stellar variability

Table 1. The comparative results of membership status of known variables of NGC 6866 has been listed here. A dotted pink line (as defined by Eq.1), is used to separate red-component stars (RCS) and blue component stars(BCS) in Fig.1.

	Joshi *et al.* (2012)					Present Study		
Star ID	Period (d)	$< V >$ (mag)	Amplitude (V-mag)	Membership status	Variable type	Period (d)	V-Amplitude (mag)	Category
0016	0.465333	11.747	0.064	Likely	Binary?	0.465462	0.082	BCS
0020	0.380373	12.003	0.032	Unlikely	Binary?	0.380264	0.042	BCS
0027	0.143616	12.222	0.039	Member	δ Scuti	0.143638	0.064	BCS
0036	0.214684	12.623	0.035	Likely	δ Scuti	0.515320	0.066	BCS
0039	0.836120	12.677	0.035	Likely	γ Doradus	0.835128	0.085	BCS
0047	0.275710	12.995	0.041	Unlikely	?	0.275606	0.079	BCS
0058	0.911577	13.246	0.052	Field	γ Doradus	0.911635	0.182	RCS
0074	0.321750	13.469	0.055	Likely	Elliptical	0.160855	0.117	BCS
0081	1.239157	13.548	0.058	Likely	γ Doradus	1.236996	0.225	BCS
0094	0.740741	13.878	0.087	Member	γ Doradus	0.739284	0.168	BCS
0158	2.285714	14.902	0.052	Member	EA	1.141031	0.089	BCS
0191	1.090513	15.285	0.085	Likely	Binary?	20.907380	0.173	BCS
0221	0.476872	15.564	0.079	Likely	PV	0.937075	0.153	**BCS**
0231	0.327547	15.615	0.052	Member	PV	0.478590	0.078	BCS
0239	37.037037	15.630	0.260	Unlikely	Semi-regular	37.778617	0.283	RCS
0248	0.437446	15.660	0.210	Likely	Elliptical	0.218657	0.166	BCS
0253	7.407407	15.730	0.060	Field	Rotational	7.554011	0.114	RCS
0332	11.494253	16.190	0.140	Field	Semi-regular	11.500862	0.237	RCS
0349	12.048193	16.310	0.100	Unlikely	Semi-regular	11.870845	0.163	RCS
0444	16.260162	16.820	0.310	Field	EB	8.115565	0.177	RCS
0487	0.415110	17.210	0.340	Member	W UMa	0.207608	0.298	BCS
0494	0.366704	17.260	0.440	Unlikely	W UMa	0.183312	0.285	**RCS**
1077	0.033559	18.580	0.340	Unlikely	HADS	0.033559	0.100	**RCS**
1088	0.184775	18.670	0.280	Field	HADS	0.184864	0.024	**RCS**
1274	0.462428	19.050	0.460	Unlikely	W UMa	0.229491	0.020	**RCS**
1292	0.295247	18.950	0.370	Unlikely	HADS	1.318235	0.022	**RCS**
1421	0.041263	19.150	0.300	Unlikely	HADS	0.041262	0.015	**RCS**
1583	0.082055	19.260	0.320	Likely	HADS	0.297459	0.012	**BCS**

Table 2. Proper motion values of the variables extracted from the Gaia EDR3 data (Gaia Collaboration et al. 2016, 2021). The distances of the variables are also computed through the parallax values, as extracted from the Gaia EDR3 data. Old membership probability (P_{sp}, P_{ph}, P_{pm}) of variables is listed as per Joshi et al.(2012).

Star ID	RA (J2000)	Dec. (J2000)	Membership Probability P_{sp}	P_{ph}	P_{pm}	Distance (kpc)	μ_α (mas/yr)	μ_δ (mas/yr)	P_{pm} (GAIA)
016	20:03:26.12	+44:10:05.3	0.28	1.00	0.66	0.748±0.008	2.751±0.013	-2.150±0.013	0.518
020	20:04:25.52	+44:10:16.2	0.19	1.00	0.16	0.420±0.169	-0.176±0.467	-3.468±0.480	0.495
027	20:03:47.13	+44:09:25.7	0.82	1.00	0.80	1.465±0.015	-1.109±0.012	-5.650±0.013	0.393
036	20:03:42.47	+44:10:06.4	0.70	0.47	0.84	1.433±0.017	-0.669±0.015	-5.798±0.015	0.384
039	20:03:54.18	+44:06:46.0	0.60	1.00	0.81	1.509±0.018	-1.328±0.013	-6.163±0.014	0.361
047	20:04:11.20	+44:05:33.3	0.27	1.00	0.55	1.443±0.017	-1.429±0.014	-5.834±0.015	0.382
058	20:03:31.61	+44:07:59.8	0.38	0.00	0.00	0.231±0.002	10.650±0.013	22.541±0.013	-1.480
074	20:03:34.93	+44:14:50.1	0.11	1.00	0.72	1.412±0.045	-1.167±0.037	-5.656±0.038	0.393
081	20:03:27.93	+44:09:19.1	0.33	1.00	0.92	1.178±0.012	-1.389±0.013	-8.366±0.012	0.200
094	20:03:59.34	+44:10:25.8	0.82	1.00	0.77	1.443±0.019	-0.590±0.015	-5.982±0.015	0.373
158	20:03:40.87	+44:09:40.0	0.66	1.00	0.75	0.951±0.015	-1.139±0.019	-9.258±0.020	0.128
191	20:03:33.48	+44:13:53.4	0.19	1.00	0.67	1.164±0.022	-0.355±0.022	6.304±0.022	0.050
221	20:03:53.35	+44:04:04.2	0.21	1.00	0.86	1.640±0.036	-2.085±0.025	-7.075±0.026	0.298
231	20:03:48.28	+44:10:56.6	0.76	1.00	0.81	1.438±0.033	-1.319±0.027	-5.609±0.029	0.396
239	20:04:19.00	+44:07:05.8	0.27	1.00	0.81	10.162±0.149	-3.310±0.016	-3.004±0.019	0.507
248	20:03:38.79	+44:04:53.0	0.22	1.00	0.74	1.193±0.026	0.741±0.025	-0.107±0.027	0.485
253	20:04:20.84	+44:10:03.9	0.31	0.00	0.32	3.648±0.080	-6.613±0.025	-11.162±0.029	-0.035
332	20:03:43.64	+44:05:19.7	0.33	0.00	0.18	0.316±0.007	9.093±0.026	1.322±0.027	0.419
349	20:04:11.78	+44:13:06.9	0.32	0.00	0.97	7.757±0.209	-3.526±0.030	-4.125±0.031	0.472
444	20:04:21.25	+44:15:40.6	0.00	0.00	0.00	5.980±0.208	-2.438±0.036	-4.146±0.041	0.915
487	20:03:49.82	+44:11:08.5	0.76	1.00	0.85	3.510±0.174	-3.408±0.054	-8.080±0.055	0.223
494	20:04:00.17	+44:14:03.2	0.34	1.00	0.00	2.520±0.128	-3.223±0.055	-7.602±0.054	0.259
1077	20:04:13.87	+44:03:45.8	0.02	0.00	0.96	3.386±0.349	0.292±0.111	2.516±0.129	0.346
1088	20:03:56.20	+44:12:49.9	0.53	0.04	0.03	6.297±0.709	-2.642±0.128	-5.713±0.132	0.389
1274	20:04:26.66	+44:05:35.9	0.00	1.00	—	6.067±0.882	-2.264±0.156	-5.150±0.185	0.422
1292	20:03:41.23	+44:12:17.9	0.49	0.30	0.98				
1421	20:03:41.08	+44:08:47.4	0.65	0.00	1.00	-15.174±2.217	-2.128±0.170	-2.354±0.177	0.517
1583	20:03:58.70	+44:11:33.5	0.70	0.00	0.73	2.394±0.373	-6.195±0.178	-6.601±0.189	0.332

of cluster members is most effectively used to constrain the models of stellar evolution and pulsation processes. Thus, the basic properties of variables can also be derived from the properties of their associated cluster (Mowlavi *et al.* 2013). The simultaneous CCD photometry of variables and comparison stars in the cluster enables us to obtain more precise time-series analysis data by observing the stars under the same weather and instrumental conditions (Kim *et al.* 2001). To this end, we have identified a suitable candidate cluster, NGC 6866, to carry out a membership study of variables within its periphery. A total of 28 variables have been identified in the analysis of Joshi *et al.*(2012) within the core region of NGC 6866. A total of 768 frames of time series observations have been accumulated by them in V-band by using the 1.04-m Sampurnanand telescope at ARIES, Nainital during 29 observational nights from 26-09-2008 to 10-01-2011. They have transformed extracted stellar magnitudes into the standard V magnitudes. We use their work through the VIZIER service.

2 Membership status of variable stars

A study of identified variables of NGC 6866 has been carried out to check their membership status as described below.

2.1 Bluer and redder stars of NGC 6866

Identified stars from the target field are also assigned as bluer or redder according to their location in CMD plane with respect to the MS. Joshi (2016) proposed the following magnitude-colour relation for separating the giant stars and MS stars from the cluster through the best visual fit of isochrones on the CMD plane of MS,

$$V_o = 7.66\times(B-V)_o + 7.32, \tag{1}$$

where V_o and $(B-V)_o$ are the observed magnitude and colour of stars. If, V_o value of a star satisfies the expression V_o>$7.66\times(B-V)_o + 7.32$, then it will be a bluer member of the studied cluster. The group of such bluer members defines the blue component stars (BCS) of a cluster, which are lying on the left side of main sequence (MS) of the $(B-V)$ vs V CMD of the studied cluster. Similarly, the group of red component stars (RCS) is laying on the right side of the MS of the above CMD. These redder members satisfy a condition of V_o≤$7.66\times(B-V)_o + 7.32$.
The prescribed linear relations are only applicable for the V-magnitude range from 10-mag to 18.5 mag. Separating lines of the BCS and RCS regions are depicted by pink dotted line in Fig.1 and stellar sequences of the cluster's MS and giant stars are visually separated from each other within the above mentioned range. The $(B-V)$ vs V CMD shows merger of both these sequences for the fainter stars with $V-mag \geq 18.5$ and the above linear relations are not applicable for them.

2.2 Membership status of Variables

Joshi *et al.* (2012) assigned various membership probabilities for the variables according to their spatial (P_{sp}), photometric (P_{ph}) and kinematic (P_{pm})

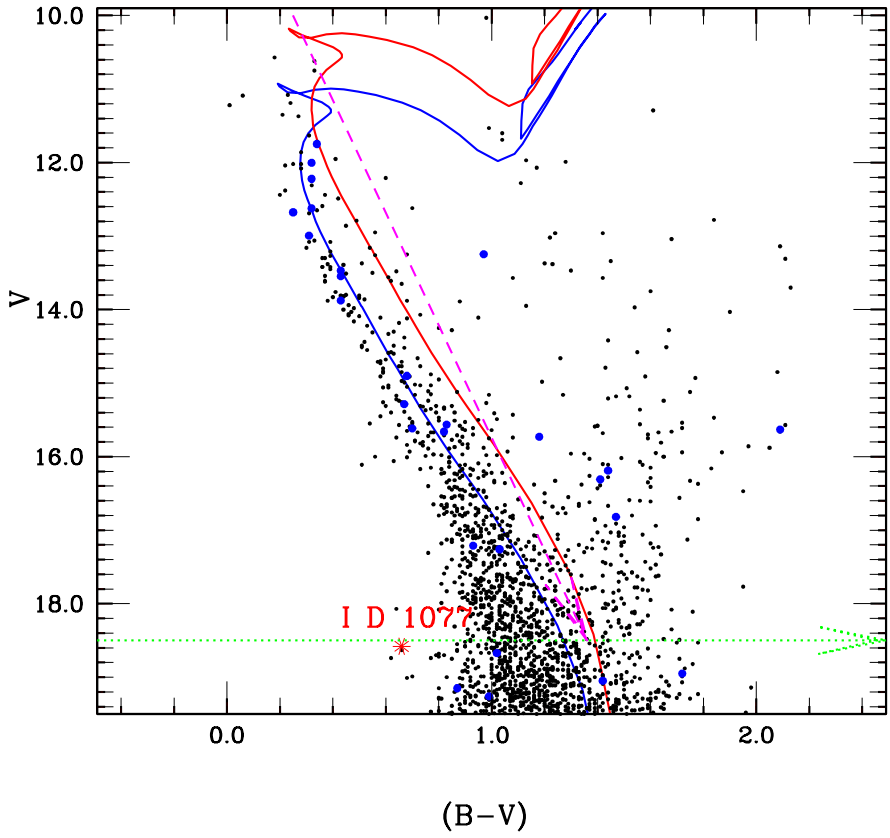

Fig. 1. The $(B-V)$ vs V CMD of stellar members of NGC 6866 with Variables. Stellar variables are depicted by blue dots. The intrinsic values V_0 and $(B-V)_0$ of Eq.1 are converted into absolute values of the observational plane V vs $(B-V)$ by colour-excess, $E(B-V) = 0.12$. Eq.1 is drawn as a dashed pink line on the CMD. Blue and red isochrones represent the blue and red envelope of the cluster MS. A dotted green line represents the limit above which it is not possible to separate groups of BCS and RCS into the main sequence of cluster.

probabilities. They have chosen these stars as cluster members either due to photometric probability $P_{ph} = 1$, or due to proper motion criteria, i.e. kinematic probability ($P_{pm} > 0.6$). According to them, unlikely members are those stars which satisfy only one criterion and belong outside of the core-region ($P_{sp} < 0.71$) of the cluster. Using 3σ clipping algorithm for confirmed photometric probabilistic members ($P_{ph} = 1$), the mean proper motion values of NGC 6866 are found to be -1.938 ± 0.088 mas/yr and -4.842 ± 0.134 mas/yr in Right Ascension(RA) and declination(DEC), respectively. The standard deviation values (σ_α, σ_δ) of proper motion of stars of NGC 6866 are found to be 1.840 and 2.803 in RA and DEC, respectively. These values give resultant standard deviation $\sigma = \sqrt{\sigma_\alpha^2 + \sigma_\delta^2} = 3.353$. Joshi et al.(2012) computed proper motion probability as per Kharchenko et al.(2004) for each variable star, which gives approximately 0 probabilistic values for Gaia data.
The author assumed that the stars, lying within 3σ limit of the mean proper motion of the cluster members, are kinematic members of the cluster. The proper motion probability is assigned to be 1 for stars having coincident proper motions with the cluster, whereas the proper motion probability is assigned to be 0 for stars having proper motions outside the 3σ limit. Negative proper motion probabilities are found for field stars (ID 058 and 253). Proper motion probability of other member stars is computed as $P_{pm} = 1 - \frac{\sqrt{(\mu_\alpha - \bar{\mu_\alpha})^2 + (\mu_\delta - \bar{\mu_\delta})^2}}{3\sigma}$.

2.3 Comparison of membership status of variables

In the view of comparative study of membership of variables, having $V - mag \leq 18.5$, we conclude the following:
1) All members and likely stellar variables of NGC 6866 belong to the BCS category, whereas all field variables are members of the RCS family.
2) Unlikely members may be either BCS or RCS. Those unlikely variables classified as BCS were selected through the photometric criteria, whereas others are RCS.
3) The proper motion distribution of the BCS and RCS of NGC 6866 shows no separation pattern (Joshi, 2016), therefore the kinematic probabilities give no result to show them as BCS and RCS.
4) Due to the CMD photometric broadening and merging of sequences of the giant stars with the cluster MS at the end of the fainter stars ($V - mag \geq 18.5$), there is no direct visual evidence to separate such faint stars into BCS and RCS.
5) Joshi(2016) has calculated the heliocentric distance for the NGC 6866 cluster as 1.19 ± 0.04 kpc. The distance values of star IDs 081, 191 and 248 also closely match this (listed in Table 2). The distances of eight stars, having IDs 027, 036, 039, 047, 074, 094, 158 and 231, are within 30 percentage uncertainty range of the cluster's distance from us. All these stars are BCS.

Thus, we have classified faint variable stars as BCS and RCS according to the photometric, spatial criteria of membership. They are listed in Table 1.

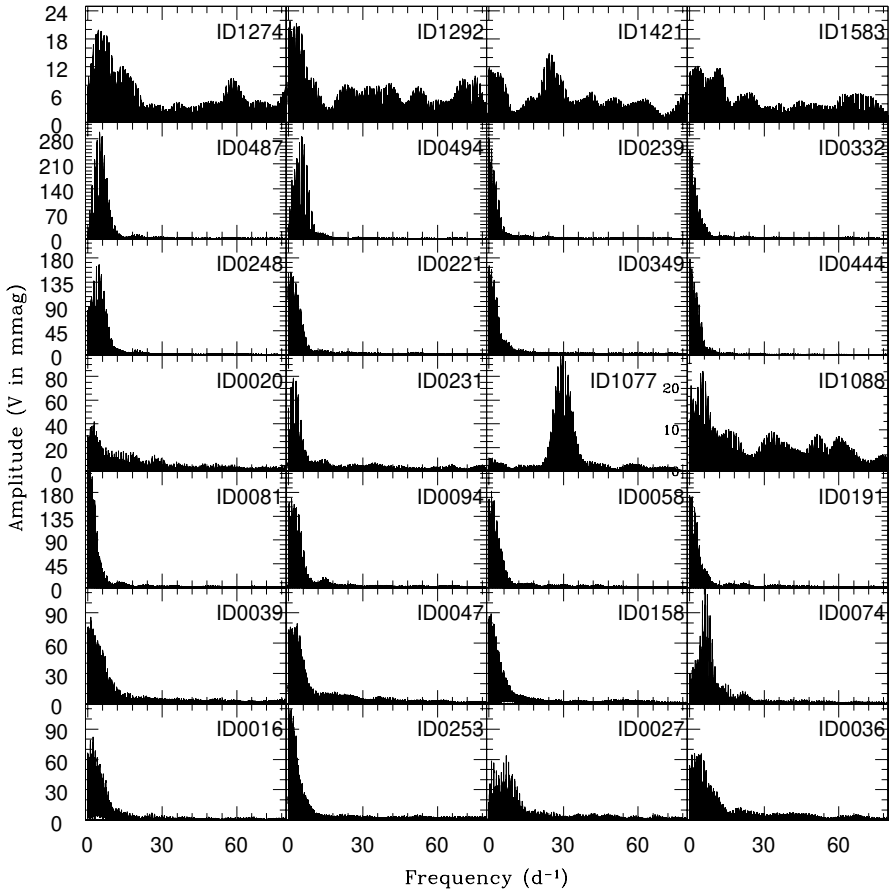

Fig. 2. The power spectrum of variable stars in the range of 0 to 79.8 d^{-1}. The X-axis and Y-axis represent the frequency (d^{-1}) and amplitude (mmag) in the V-band, respectively.

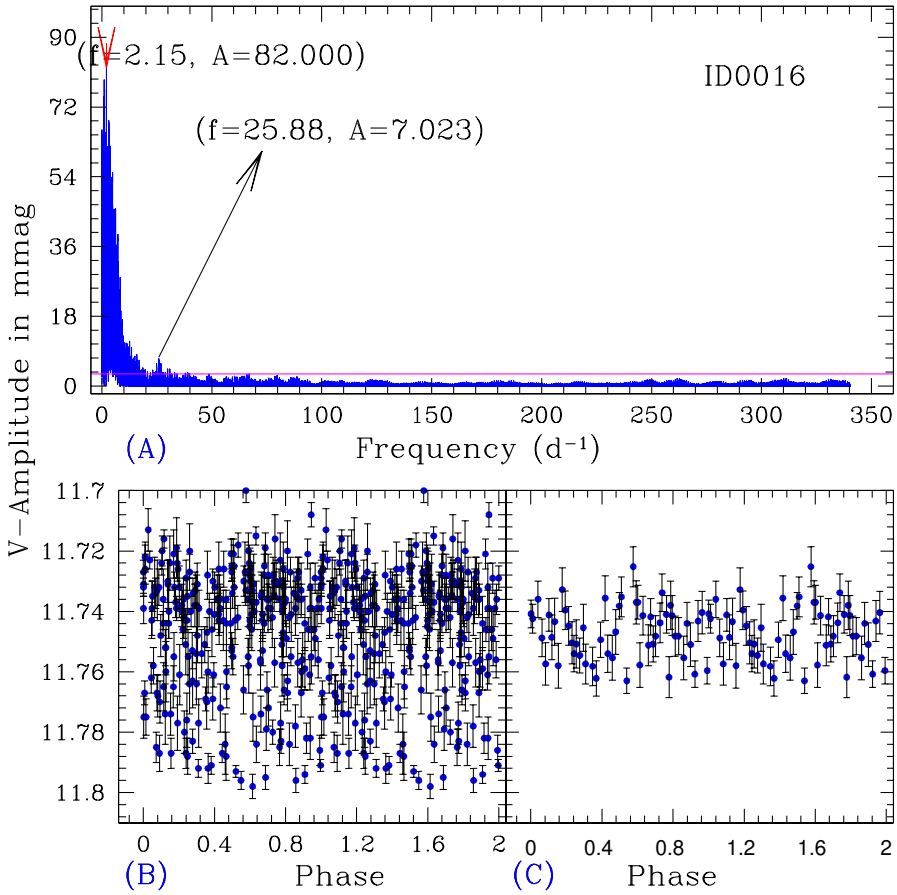

Fig. 3. (A) The frequency spectrum of the variable star ID 0016 (Range:0-360 cd^{-1}). The X-axis and Y-axis represent the frequency (d^{-1}) and amplitude in the V-band (mmag), respectively. **(B)** The phase diagram of the variable ID 0016 of NGC 6866 is depicted by the original data-points for frequency, 2.15 cd^{-1}, as extracted from the VizierR service. **(C)** The phase diagram of variable ID 0016 of NGC 6866 for frequency 2.15 cd^{-1}, after binning each of the 5 data-points of extracted data.

3 Motivation to analysis of frequency spectrum

A temporal analysis of the frequency spectrum is a valid method to find out the periodicity of variables. Such analysis provides information about physical phenomena and stellar nature for the variable stars. Therefore, we constructed the frequency spectrum by running the PERIOD-4.0 program (Lenz & Breger 2005) on the extracted data file of each variable star. The frequency spectra of the variable stars are shown in Fig.2.

Such frequency spectrum has many asymptotic parabolic functions (any-Gaussian, Shannon's function, etc.) and they arise due to the interaction of stellar pulsations, instrumental errors and noise. The corresponding frequency of the peak of each pattern is known as potential value of pulsation for the variable. The highest peak above the 3σ level in the spectrum is known as the amplitude of the pulsation and the corresponding frequency is known as the pulsation frequency (f_0) for the variable. The revised results of periods and amplitudes of the 28 variables of NGC 6866 are listed in Table 1 along with the literature results. A comparative analysis of new revised results and literature results shows dissimilarities from each other, which has led us to research the precise stellar pulsations for the known variables of NGC 6866.

4 Phase and smoothness of the phase diagram

A phase of the variable is a scale measurement in terms of cyclic variation and depends on the duration of the cyclic variation. It is not possible to take any peak above the noise level as clearly as a pulsation frequency, without realizing that some may be aliases of each other and that the low frequency range of the spectrum may play an important role in producing the spurious log periods. The phase of each data point of the light curve of a variable is computed as,

$$Phase = \ Decimal\ part\ of\ (T - T_0) \times f, \tag{2}$$

where T, T_0 and f are the HJD time of the observation epoch, the initial HJD time (JD_0) and the computed frequency of stellar variability. In the study of Joshi *et al.* (2012), the JD time for the first observed science frame of V-band of NGC 6866 on the date 26 September 2008 is given to be 2454736.088461. Since the earth is constantly changing its positions due to its orbital motion, there is a time shift during the observation of an event. To correct the time shift of observations, heliocentric Julian Date (HJD) time was applied instead of JD time. The corresponding HJD time for the first epoch of the present study is 2454736.09049 and we found a time shift of 2.916 minutes. The resultant decimal part is arranged in ascending order. As a result, the cyclic variation of the variables overlap with each other in a single phase-folded diagram with scattered data points. In order to gradually reduce the scattering and improve the smoothness of the phase diagram, binning procedure and average moving procedure are applicable. Pulsation amplitude also decreases with an increment of smoothness. A comparative analysis of both procedures carried out for variable ID 0016 of NGC 6866 is described below.

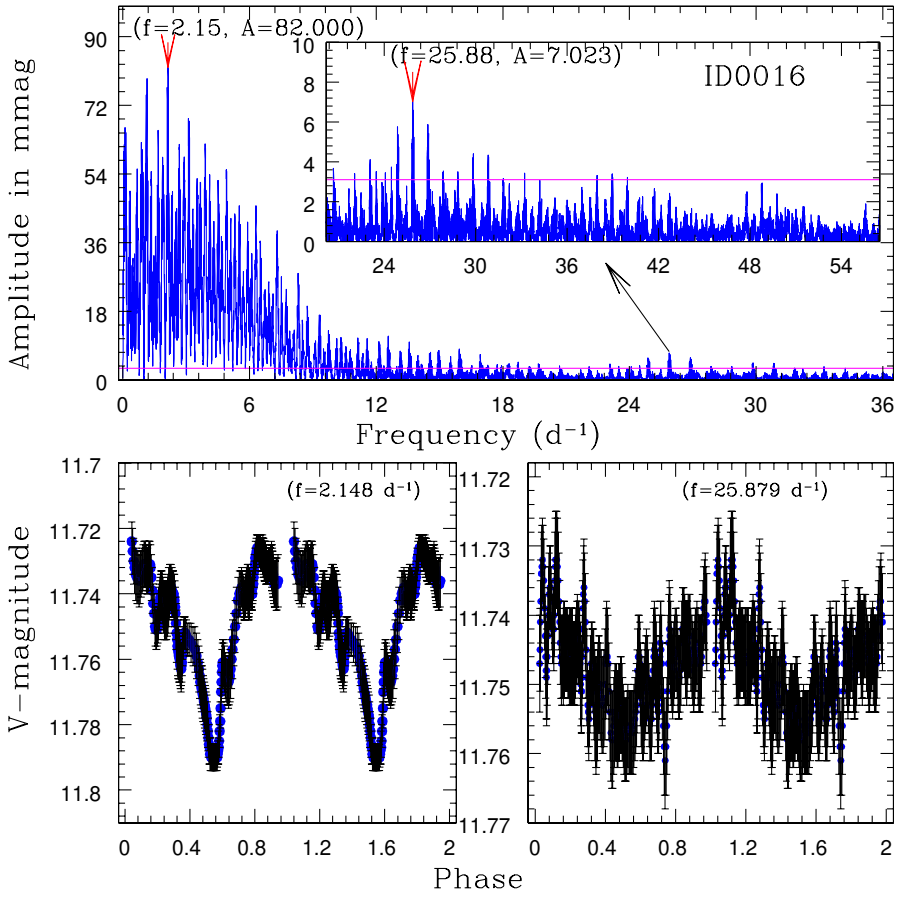

Fig. 4. In the upper panel, we have shown the frequency spectrum of the variable star ID 0016. In the lower panels, the phase diagrams of ID 0016 are depicted for the two frequencies, namely 2.15 cd^{-1} and 25.88 cd^{-1}.

4.1 Used procedure for smoothing of phase diagrams

A typical frequency spectrum of NGC 6866 cluster's binary variable star system, ID 016, is depicted in Fig. 3 and 4. In these figures, the amplitude within a frequency domain of its power spectra is continuously decreasing from 2.15 cd^{-1} to 20 cd^{-1}. In the remaining part of its frequency spectrum, the highest peak is detected at 25.88 d^{-1} through visual inspection. The corresponding amplitude peak of the 25.88 cd^{-1} frequency was found to be approximately 7 $mmag$. It exceeds the 3σ limits compared to peaks in all other remaining parts of the high-frequency spectrum. Such amplitudes (in order of $3-4$ $mmag$) are alias frequencies due to the interaction of instrumental errors and noise. Thus, the spectrum's frequency of 25.88 cd^{-1} (with a peak of 7 $mmag$) becomes an interesting frequency to position it as an additional pulsation. The phase diagrams of both the frequencies (2.1484 cd^{-1} and 25.8787 cd^{-1}) are shown in Fig. 4.
The frequency spectrum of NGC 6866 cluster's variable ID 0016 is depicted in Fig.3(A). The highest amplitude of pulsation, $f_1 = 2.15cd^{-1}$, has been computed to 82 mmag and the corresponding phase diagram is shown in Figure 3(B) through the original data-set as extracted from the VizieR service. In Figure 3(C), we have shown the phase diagram of studied stellar variable after binning each of the 5 successive data-points of phase. In the above prescribed phase diagram, the amplitude has been computed as 44 mmag, i.e., 53.66 percent of the original computed amplitude.
The moving average procedure is also used in the construction of the smoothed phase diagram of ID 0016 and the resulting phase diagram of $f_1 = 2.148 \simeq 2.15cd^{-1}$, as shown in the lower left panel of Fig.4. The amplitude of this phase diagram is calculated to be approximately 68 mmag, i.e. 82.93 % of the original calculated value of the amplitude. These results show a decrement rate of amplitude via the binning procedure of data points that is comparatively higher than the one, obtained via moving average procedure. Obviously, the light curve shows an eclipse-like narrow trough for pulsation, 2.15 cd^{-1} due to the presence of harmonics of the main frequency (4.3 cd^{-1}) and its amplitude seems larger than the "fast variations". Similarly, an interesting peak is found at $f_2 = 28.88cd^{-1}$ in the frequency spectrum. It has an amplitude of 26 $mmag$ and its corresponding phase diagram is shown in Fig.3. The peak of $f_1 = 2.15cd^{-1}$ is comparatively higher than the peak of $f_2 = 28.88cd^{-1}$. The value of f_2 is 13.43 times that of f_1. It confirms that f_2 is not harmonic of f_1. Thus, f_2 can become an additional pulsation frequency for variable ID 0016.

5 Validity test for known HADS stars

A total of five High Amplitude Delta Scuti (HADS) variables have been reported by Joshi *et al.* (2012) within NGC 6866. Their IDs are 1077, 1088, 1292, 1421 and 1583. The author performed a validity test of their characteristics as HADS. Generally, HADS variables are late A and early F type pulsating stars and they change their absolute magnitude and radial velocity over a period of one to six hours. The amplitude of HADS should be greater than 0.2 mag (Breger & Montgomery 2000). The relationship of the period and absolute

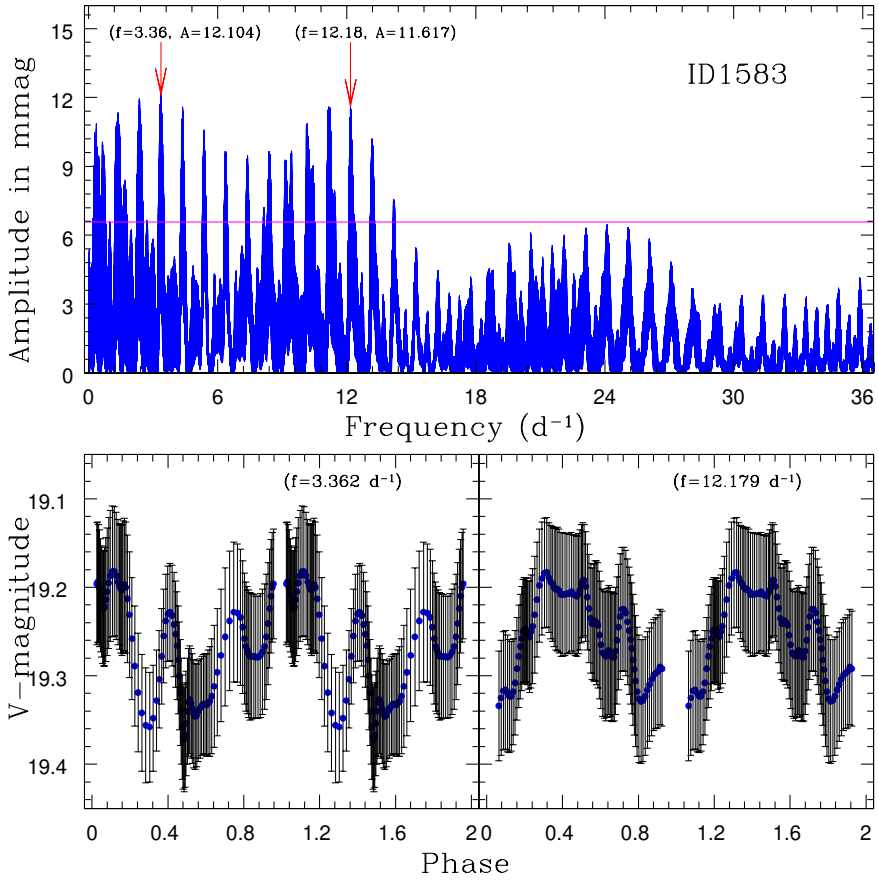

Fig. 5. Frequency spectrum of the variable star ID 1583 in the lower frequency domain. The X-axis and Y-axis represent the frequency(d^{-1}) and amplitude in the V-band, respectively. The pink line represents a value of 6.5 *mmag* as detected through analysis of the frequency spectrum of a sample of known HADS stars in the region of high frequencies. In the lower panels, the phase diagrams of variable ID 1583 are depicted for the two frequencies, namely 3.36 cd^{-1} and 12.18 cd^{-1}.

magnitude of Delta-Scuti stars is given as (McNamara 2011):

$$M_V = (-2.89\pm0.13) log\ P - (1.31\pm0.10), \quad (3)$$

where M_V and P are the absolute magnitude and period of the Delta-Scuti stars. It is also applicable for the HADS stars (Salmanzadeh *et al.* 2015). McNamara (2011) also provides a relation for $(B-V)_o$ and period as:

$$(B-V)_o = (0.105\pm0.004) log\ P + (0.336\pm0.005), \quad (4)$$

where $(B-V)_o$ is the colour-index.

All of these stars have an observational $(B-V)_0 > 0.60 mag$, three of them exceeding 1 mag (Table 3). Since HADS are A-F spectral type, MS (or slightly more evolved) stars, and have $(B-V)_0 < 0.50\ mag$, the characteristics of known HADS stars of NGC 6866 (Joshi *et al.* 2012) do not fit with the characteristics of the standard HADS variables.

The estimated values of the model absolute magnitudes and $(B-V)_0$ of the

Table 3. Model values of absolute magnitude and colour-excess for different HADS stars.

Star ID	$log\ P_{ef}$ (days)	M_V (Mo.)	$(B-V)_o$ (Mo.)	M_V (Ob.)	$(B-V)_o$ (Ob.)
1077	-0.474	0.060	0.286	7.83	0.66
1088	-0.733	0.808	0.259	7.92	1.02
1292	-0.639	0.537	0.269	8.20	1.72
1421	-1.384	2.691	0.191	8.40	0.87
1583	-0.527	0.212	0.281	8.51	0.99

sample HADS have been found to be far from the calculated values of a sample members through CMD analysis of the NGC 6866 cluster. Thus, the sample stars have no confirmed membership of the studied cluster.

5.1 Specific comments on the variable ID 1583

ID 1583 is a fainter detected variable star in the field of NGC 6866. Its study is beneficial for understanding the nature of the cut-off frequency and for determining the pulsation of similar fainter variable stars through analysis of the frequency spectrum of ground based observations. For this purpose, we have taken the first four asymptotically parabolic patterns of frequencies from its frequency spectrum. The peak of all other asymptotically parabolic patterns is below 6.5 mmag, which is depicted by a solid red line in the upper panel of Fig.5. In the lower frequency domain of its spectrum, the conjugate asymptotically parabolic patterns show almost identical peaks for the twin frequencies (3.36 $cd^{-1} \simeq f_1$ and 12.18 $cd^{-1} \simeq f_2$). Their phase diagrams are shown in the lower panel of Fig.5. Its new periodic value, 12.18 cd^{-1}, matches with the estimated value by Joshi *et al.* (2012). The value of f_2 was found to be 3.6 times that of f_1, which means that f_2 is not an overtone of f_1. The

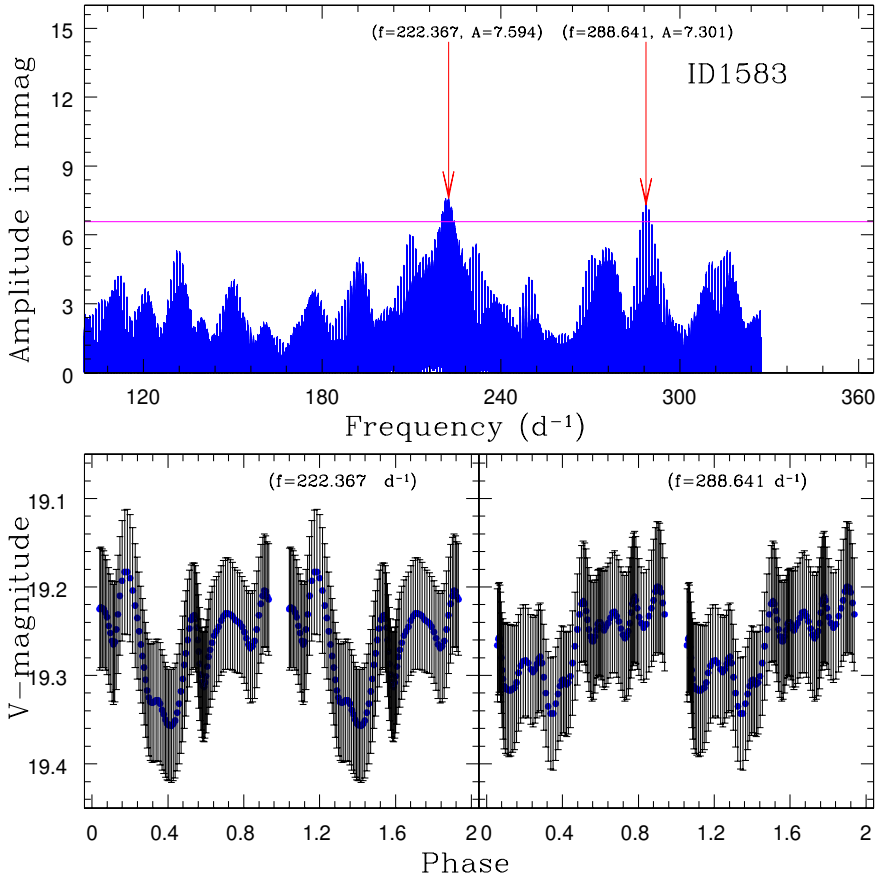

Fig. 6. Frequency spectrum of the variable star ID 1583 in the high frequency domain. The X-axis and Y-axis represent the frequency(d^{-1}) and amplitude in the V-band, respectively. The power spectrum of the higher spectral window does not show full cycle pulsation and confirms the importance of the limitation of temporal resolution. The pink line's meaning is discussed in Fig.4. In the lower panels, the phase diagrams of the variable ID 1583 are depicted for two frequencies, namely 222.37 cd^{-1} and 288.64 cd^{-1}.

amplitude and smoothness of the phase diagram of f_1 is found to be higher than that of the phase diagram of f_2. As a result, f_1, instead of f_2, is selected as the main pulsation frequency for the variable ID 1583.
The positions of other frequencies (222.367 $c\ d^{-1} \simeq (f_3)$ and 288.641 $c\ d^{-1} \simeq (f_4)$) within the high frequency domain of ID 1583 and their phase diagrams are shown in the upper and lower panels of Fig.6, respectively. Phase diagrams of f_3 and f_4 were found to be cyclic and non-cyclic, respectively. They do not have the overtones of f_1 and f_2. Furthermore, frequencies above $100cd^{-1}$ can hardly be detected in the best quality space data or in very fast ground based photometry. Thus, it is physically impossible to identify such high frequencies (f_3 and f_4) and therefore are considered to be instrumental errors in nature.

5.2 ID 1077: is a SX Phoenicis variable ?

The HADS stars are fainter members of the δ-Scuti stars (i.e. Dwarf-Cepheid). Dwarf-Cepheids are also a sub-group of Classical Cepheids. Most Classical Cepheids (CCs) are monoperiodic, although stars pulsating in an overtone are more luminous and larger than a fundamental mode pulsator with the same period (Bono *et al.* 2001). For variables such as Cepheids, a linear relationship of their stellar age and pulsation is given below (Joshi & Joshi 2014):

$$log(Age) = 8.60 \pm 0.07 - (0.77 \pm 0.08)\ log\ P, \tag{5}$$

where P is the period of the Cepheid. However, this linear relation is not applicable for ID 1077.

Observed Characteristic properties of variability: As per the PPMXL catalogue (Roeser et al. 2010), the proper motion values for ID 1077 are $-1.2 \pm 5.6\ mas/yr$ and $-2.3 \pm 5.6\ mas/yr$ in RA and DEC, respectively. These values give the tangential velocity of variable ID 1077 as $5.33 \pm 11\ Km/s$. The pulsation amplitude of ID 1077 is approximately equal to 0.1 mag, whereas, the pulsation amplitude of HADS stars is found to be greater than 0.3 mag at V-band, i.e. $\nabla m_V > 0.3\ mag$ (Breger & Montgomery 2000). Furthermore, it was detected as blue straggler star due to its spatial position in the CMD plane of NGC 6866 and is shown by red Asterisk on Fig.1. Due to the above reasons, variable ID 1077 should not be classified as a HADS. Due to its similar characteristics with δ-Scuti variables, we looked for its connection with the variable family closest to $HADS$. Most SX Phe stars also have properties similar to HADS, but not vice versa. In addition, all known SX Phoenicis variables of globular clusters are blue straggler stars (Jeon *et al.* 2004). In light of the results and the facts above, we find that variable ID 1077 is similar to SX Phe type stars.

Cluster membership status: The period of ID 1077 was computed as 0.033559 d by Joshi *et al.*,(2012) and is also verified by the present analysis. Its log(age) is calculated as 9.73 ± 0.12 yr through the age-period relation for HADS (Joshi & Joshi, 2014). The estimated log(age) of NGC 6866 cluster is 8.85 yr by Joshi(2016). As a result, the log(age) of the studied variable is

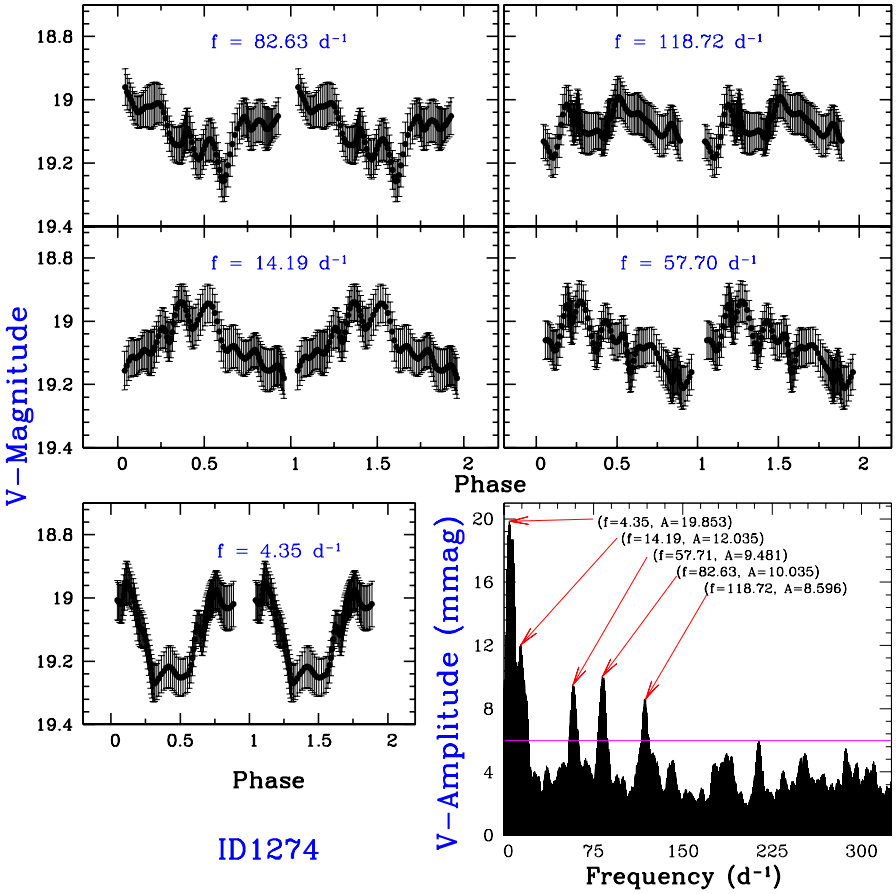

Fig. 7. The frequency spectrum and five examined pulsation frequencies of ID 1274.

greater than the log(age) of associated cluster and leads by 0.88 in the logarithm scale ($\sim$ 4662.371 Myr). It is impossible for any star to to be older than its parental cluster due to stellar formation from the same molecular cloud. The reddened value of the colour $(B-V)$ of this variable is 0.66 mag (Joshi *et al.*, 2012). Along the direction of sight of NGC 6866, the computed value of reddening, $E(B-V)$, is 0.12 mag (Joshi, 2016) and it gives the value of $(B-V)_o$ as 0.55 mag for ID 1077. This value is far from the Zero-Age-Main-Sequence (ZAMS) condition of the NGC 6866 cluster. Thus, we find that variable ID 1077 is not a member of NGC 6866 cluster.

Confirmation of SX Phoenicis status based on characteristics: The periodic values of the SX Phoenicis variables are within time scales of 0.03-0.08 days, therefore, the estimated value of the period of ID 1077 satisfies the short period pulsation characteristics of the SX Phe variables. It is defined as a low mass star due to its fainter limits in the CMD plane of NGC 6866. Since the mass-range of SX Phe variables is defined as 1.0-1.1 $M_{\odot}$ (Fiorentino *et al.* 2014), variable ID 1077 seems to be a SX Phe star due to its estimated mass. In the CMD plane of the studied cluster, SX Phe variables are bluer (with higher temperature) than main sequence stars with similar luminosity and magnitude (Santolamazza *et al.* 2001). This fact is also verified for variable ID 1077 due to its spatial position in the CMD plane of NGC 6866. Thus, the variable ID 1077 shows the properties required to define the SX Phoenicis variables. For this reason, it is classified as SX Phoenicis type. Since SX Phe stars belong to the old Galactic disk population, presence of such star in the open cluster is unlikely. In the case of ID 1077, it has an unlikely membership of NGC 6866 cluster (Joshi *et al.*, 2012) and does not lie on the main sequence of the studied cluster. Similarly, our present analysis also indicates that variable ID 1077 is not a confirmed member of the open cluster, NGC 6866. Consequently, we conclude that ID 1077 does not lie within the periphery of NGC 6866 and that it may be located within the Galactic Halo region.

6 Validity test for higher frequencies

The value of Nyquist frequency should be a good estimate for the upper frequency limit due to the sampling pattern for the current data set. The minimum time interval of two successive data points is found to be 1.724×10^{-3} d. This value gives the Nyquist frequency as 290 cd^{-1}. Frequency analysis of ID 1583 also confirms no noticeable peak value above 290 cd^{-1}. Such analytic results of high frequencies of ID 1583 motivated **the** author to investigate the nature of such frequencies for other variables, namely, ID 1274, ID 1421 etc. due to similar characteristics as shown in Fig.2. As a result, their frequency spectra (range $0-360cd^{-1}$) are depicted in Fig.7 and 8. Such analyses **are** useful to understand the nature of the spectrum for fainter variables.

6.1 Analysis of the frequency spectrum of ID 1274

The frequency spectrum of ID 1274 has five noticeable peaks in different asymptotic distributions of frequencies above the 3σ limit of the noise level,

as shown in Fig.7. The frequency of these peaks are $f_1 = 4.35cd^{-1}$, $f_2 = 14.19cd^{-1}$, $f_3 = 57.71cd^{-1}$, $f_4 = 82.83cd^{-1}$ and $f_5 = 118.72cd^{-1}$ and their corresponding amplitudes are 19.863 $mmag$, 12.035 $mmag$, 9.481 $mmag$, 10.035 $mmag$ and 8.596 $mmag$, respectively. Furthermore, the asymptotic distributions of frequencies f_1 and f_2 merge into each other and form some aliases due to their interference. To investigate the nature of the variability of these frequencies, we constructed phase folded diagrams of each said frequency as shown in Fig.7. The shape of the phase diagrams of f_1 and f_2 confirm the cyclic variation of the stellar variability. The amplitude of f_2 is 60.59 % of that of f_1 and the value of f_2 is 3.26 times that of f_1. As a result, f_2 does not have an overtone of f_1. The value of f_5 is more than $100cd^{-1}$ and is impossible to detect through the current observational facilities. As shown in Fig.5, we find no indication of stellar variability in the phase folded diagram of f_5. The values of f_3 and f_4 are less than $100cd^{-1}$ and they have well defined signatures of stellar variability. Note, that the amplitude of f_4 is more than that of f_3. The amplitudes of f_3 and f_4 are 10.29 % and 16.75 % more than that of f_5. The fitness of the phase diagram of f_3 has more distortion than that of f_4. It indicates that the signature of stellar variability gradually weakens towards the lower amplitudes of potential pulsations near the noise level of the spectrum.

6.2 Analysis of the frequency spectrum of ID 1421

In the frequency spectrum of ID 1421 we found several asymptotic distributions of frequencies, as shown in Fig.8. We have drawn a pink line such that at least one peak of the prescribed distribution of high frequencies will be found above 100 cd^{-1} and other peaks of the asymptotic distributions of high frequencies domain will lie under this line. In this regard, the value of this pink line is 6.5 $mmag$, and was reached through visual inspection of the frequency spectrum. The peak value of the distribution of high frequencies (above $100cd^{-1}$) was found at frequency $182.58cd^{-1}$, which has an amplitude of 7.42 $mmag$. In the domain of frequencies less than $100cd^{-1}$, there are two asymptotic distributions of frequencies, whose amplitudes were found to be above this line. The amplitudes of these frequencies, $3.61cd^{-1}$ and $24.23cd^{-1}$, were found to be 10.784 $mmag$ and 14.790 $mmag$, respectively. The phase diagrams of all the above frequencies are shown in the panels of Fig.8 marked as 'ID 1421'. We find no indication of stellar variability in the phase diagrams of frequencies $3.61cd^{-1}$ and $182.58cd^{-1}$. This again confirms the impossibility of detecting frequency above $100cd^{-1}$. Although the amplitude of frequency $3.61cd^{-1}$ is very high, it is characterized by instrumental error. Thus, pulsation of ID 1421 is confirmed only for the frequency $24.23cd^{-1}$.

6.3 Analysis of the frequency spectrum of ID 1088

We drew a pink line of 6.5 $mmag$ in the frequency spectrum of ID 1088, which satisfied the condition that the asymptotic distribution of frequencies with amplitude above this line had at least one peak. This peak was found at a frequency of $f_h = 192.90cd^{-1}$ with an amplitude of 7.963 $mmag$. It is marked in the domain of high frequencies of the spectrum of ID 1088 in

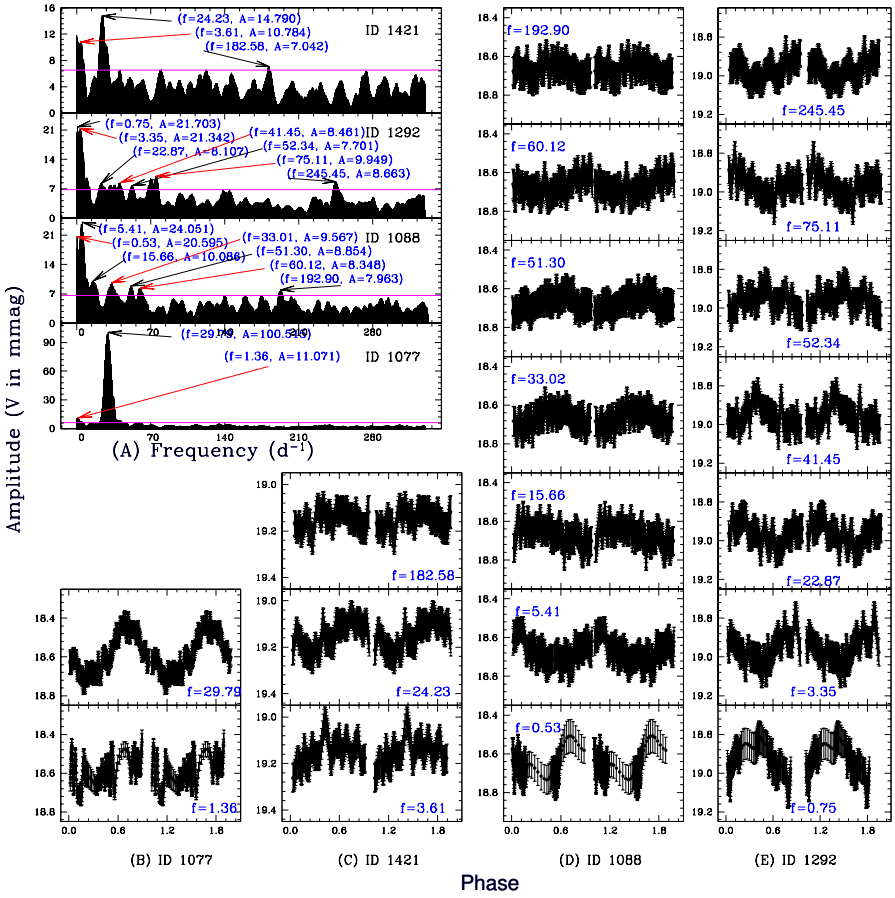

Fig. 8. The frequency spectra of the HADS stars are depicted in panel (A). In panels (B), (C), (D) and (E), are shown their respective phase diagrams for different frequencies, where a through moving average procedure is used.

Fig.8. We found six asymptotic distributions of frequencies in the spectrum of ID 1088 under $100cd^{-1}$, whose amplitudes/peaks lie above the pink line. These peaks are found at frequencies, $f_1 = 0.53cd^{-1}$, $f_2 = 5.41cd^{-1}$, $f_3 = 15.66cd^{-1}$, $f_4 = 33.01cd^{-1}$, $f_5 = 51.30cd^{-1}$ and $f_6 = 60.12cd^{-1}$ and their phase diagrams are shown in Fig.8. The corresponding amplitudes of these frequencies are 20.595 $mmag$, 24.051 $mmag$, 10.088 $mmag$, 9.567 $mmag$, 8.854 $mmag$ and 8.348 $mmag$, respectively. The phase diagrams of f_1, f_2, f_4 and f_5 show signatures of stellar variability and do not have cyclic pattern of variation of the stellar magnitudes at other frequencies. The phase diagram of f_h confirms the result of undetectable pulsation above $100cd^{-1}$ although it is easily seen by visual inspection of the phase diagram. The amplitude of these frequencies (except f_1) continuously decreases towards the higher frequencies.

6.4 Analysis of the frequency spectrum of ID 1292

We have drawn a pink line of 6.5 $mmag$ in the frequency spectrum of this variable to satisfy the following condition: at least one peak of the asymptotic distribution of frequencies must be found above this line. Such a peak of high frequencies (above 100 cd^{-1}) has been found at the frequency $245.45cd^{-1}$ with an amplitude of 8.663 $mmag$. Pulsation above 100 cd^{-1} are not expected to indicate stellar variability. In the domain of low frequencies of its spectrum below $100cd^{-1}$, we have found different peaks of the asymptotic distribution at frequencies, $f_1 = 0.75cd^{-1}$, $f_2 = 3.35cd^{-1}$, $f_3 = 22.87cd^{-1}$, $f_4 = 41.45cd^{-1}$, $f_5 = 52.34cd^{-1}$ and $f_6 = 75.11cd^{-1}$. The amplitudes of these frequencies are 21.703 $mmag$, 21.342 $mmag$, 8.107 $mmag$, 8.461 $mmag$, 7.701 $mmag$, and 9.948 $mmag$, respectively. The respective phase diagrams of these frequencies are also shown in Fig.8. After a deep inspection of these phase diagrams, we found indications of stellar variability for f_1 and f_2.

6.5 Analysis of the frequency spectrum of ID 1077

We find no indication of an asymptotic distribution in the domain of higher frequencies. However, two significant asymptotic distributions were found in the domain of the lower frequencies. These are $f_1 = 1.36cd^{-1}$ and $f_2 = 28.79cd^{-1}$ and their amplitudes are 11.071 $mmag$ and 100.511 $mmag$, respectively. The frequency spectrum and phase diagrams of ID 1077 are also depicted in Fig.8. Since the phase diagram of f_1 shows no confirmed indication of stellar variability, it may be due to either instrumental error or signal-noise.

7 Conclusion

The comprehensive membership study of a sample of variables indicates that the RCS group represents unlikely cluster members and field variables, whereas, the BCS group represents confirmed members and likely members of NGC 6866.

The frequency spectrum of any of the variables has many asymptotic distributions of frequencies in different ranges. Each asymptotic distribution has its own characteristic amplitude and the main pulsation of any variable is

the largest peak in these amplitudes. However, it is currently impossible to detect pulsations of high frequencies (above 100 cd^{-1}) through any observational facilities. A temporal analysis of frequency spectrum above 100 cd^{-1} of the current sample of variables was performed to detect the largest amplitude of regular fluctuations within the spectrum for signals of aliases/noise .

Classification of variables is a crucial task and depends heavily on observing the shape of their light curves/phase folded diagrams. Consequently, the smooth shape of these curves is required to define the type of stellar variability. The smoothing of the light curves can be achieved through either the binning procedure or the moving average procedure on the actual data points. A temporal analysis of data for ID 0016 of NGC 6866 indicates that the moving average procedure is more effective than the binning procedure.

The shape of the phase folded diagrams is also utilized to inspect the independent pulsation frequencies of a variable due to the regular shape of light-curves of regular stellar variability. The phase diagram of 118.72 cd^{-1} of ID 1274 shows no regular shape of variability. Consequently, it can not be considered as a pulsation frequency, although it has a sufficiently high amplitude compared to other neighbourhood asymptotic distributions of frequency spectrum due to aliases/ noise of signals. In the case of ID 1583 of NGC 6866, twin frequencies of pulsation have been identified in the domain of low frequencies of its spectrum, while the detected twin frequencies above $100cd^{-1}$ are noticeable potential overtones for regular pulsation due to instrumental error and noises. Such pulsation frequencies can produce pseudo or alias frequencies below $100cd^{-1}$ of spectrum such as the frequency 75.11 cd^{-1} of ID 1292, and the frequencies 15.66 cd^{-1} and $60.12cd^{-1}$ of ID 1088. Due to aliases and noise signals, there is no indication of regular stellar variability. Thus, phase folded diagrams provide supplementary results for identifying the real pulsations of regular variables.

The McNamara(2011) relations provide the resulting model values of colour $[(B-V)_o]$ and absolute magnitude of the HADS stars in the sample. These values do not match with their computed values through the best visually fitted isochrone on the CMD plane of the cluster. Thus, these stars are not considered members of NGC 6866. The variable ID 1077 seems to be a SX Phoenicis variable instead of HADS. Its postilion is in the line of sight of NGC 6866 and is located in the Galactic Halo region.

Acknowledgement

This research has made use of the VizieR catalogue access tool, CDS, Strasbourg, France. The original description of the VizieR service was published in A&AS 143, 23. This work has also made use of data from the European Space Agency (ESA) mission *Gaia* (https://www.cosmos.esa.int/gaia), processed by the *Gaia* Data Processing and Analysis Consortium (DPAC, https://www.cosmos.esa.int/web/gaia/dpac/consortium). Funding for the DPAC has been provided by national institutions, in particular the institutions participating in the *Gaia* Multilateral Agreement.

References

Bono, G., Gieren, W. P., Marconi, M., Fouqué, P., 2001, ApJ, 552, 2
Breger, M., Montgomery, M.H., 2000, APS Conf. ser., 210, 3
Briquet, M., Hubrig, S., De Cat, P., Aerts, C., North, P., Schöller, M., 2007, A&A, 466, 269
Derekas, A., Kiss, L. L., Székely, P., et al., 2009, MNRAS, 394, 995
Eyer, L. & Mowlavi, N., 2008, J. Phys. Conf. Ser., 118, 012010
Fiorentino, G., Lanzoni, B., Dalessandro, E., et al., 2014, AJ, 783, 34
Gaia collaboration et al., 2016, A&A, 595A, 2
Gaia collaboration et al., 2021, A&A, 649, A1
Gautschy, A. & Saio, H., 1996, ARAA, 34, 551
Jeon, Young-Beom; Lee, Myung Gyoon; Kim, Seung-Lee; Lee, Ho, July 2004, AJ, 128 (1), 11
Joshi, G.C., 2016, Advances in Computer Science and Information Technology (ACSIT) ,03, 64
Joshi, Y.C., Joshi, S., Kumar, B., Mondal, S., Balona, L.A., 2012, MNRAS, 419, 2379
Joshi, Y.C., Joshi, S., 2014, New Astronomy, 28, 27
Kharchenko N. V., Piskunov A. E., Roeser S., Schilbach E., Schola R.-D., 2004, Astron. Nachr., 325, 740
Kim, S.-L., Chun, M.-Y., Park, B.-G., Lee, S. H., Sung, H., Ann, H. B., Lee, M. G., Jeon, Y.-B., Yuk, I.-S., 2001, A&A, 371, 571
Lenz, P., Breger, M., 2005, CoAst, 146, 53
Liu, L., Chen, W.P., Qian, S.B., Chuang R.J., Jiang, L.Q., Lin, C.S., and Hsiao, H.Y., 2015, AJ, 149, 111
McNamara, D. H., 2011, AJ, 142, 110
Mowlavi, N., Barblan, F., Saesen, S., Eyer, L., 2013, A&A, 554, A108
Roëser, S., Demleitner, M. & Schilbach, E., 2010, AJ, 139, 2440
Salmanzadeh, E., Zandian, S., Hasanzadeh, A., Zahabi, S., 2015, New Astronomy, 37, 76
Santolamazza, P.; Marconi, M.; Bono, G.; Caputo, F.; Cassisi, S.; Gilliland, R. L., 2001, AJ, 554 (2), 1124